Primljen / Received: 7.5.2024.
Ispravljen / Corrected: 4.9.2024.
Prihvaćen / Accepted: 12.9.2024.
Dostupno online / Available online: 10.11.2024.

# Analysis of lateral shear performance of side-toothed hollow slab based on cohesive force constitutive simulation

Authors:

Songgang Yang, MCE
1903929701@qq.com

Prof. Xiaojuan Shu, PhD. CE
254528003 @qq.com
**Corresponding author**

Yongguang Li, MCE
1600541101 @qq.com

Prof. Mingyan Shen, PhD. CE
511272252 @qq.com

Prof. Chao Zhao, PhD. CE
1020173@hnust.edu.cn

Hunan University of Science and Technology
Faculty of Civil Engineering
Xiangtan, China

Research Paper

Songgang Yang, Xiaojuan Shu, Yongguang Li, Mingyan Shen, Chao Zhao

## Analysis of lateral shear performance of side-toothed hollow slab based on cohesive force constitutive simulation

Herein, based on mortise–tenon hollow slabs, a side-toothed hollow slab structure is proposed for easier lateral connections. Side-tooth structures of both the V- and W-side teeth were constructed. By conducting shear tests on small specimens with different side-tooth shapes, a cohesive constitutive model of epoxy adhesive, which was selected as the inter-tooth bonding material, was developed. The bonding interface was simulated with a zero-thickness epoxy adhesive by using the Voronoi mathematical model for random unit division. A plane micromechanical finite element simulation model was developed using the Abaqus software to analyse the failure modes and shear strength of the hollow slabs with two side-tooth structures under shear action, and the corresponding shear tests were conducted for verification. In the V-side teeth structure, the outer concrete lost its strength earlier and exited the work process, with the height of the cracking shear surface at complete failure being approximately half of the beam height. The W-side teeth joint structure did not exhibit a significant early strength loss during shearing, with the complete shear failure surface being approximately 4/5 of the beam height. The simulation analysis showed larger crack widths during failure in the former and smaller widths in the latter.

**Key words:**
side-toothed hollow slab, shear resistance, cohesive force, finite element, simulation experiment

Prethodno priopćenje

Songgang Yang, Xiaojuan Shu, Yongguang Li, Mingyan Shen, Chao Zhao

## Analiza bočnoga posmika šuplje ploče s bočnim zupcima na temelju konstitucijske simulacije kohezijske sile

U ovom se radu, na temelju šupljih ploča sa spojem s čepom i rupom, predlaže šuplja ploča s bočnim zupcima za lakše bočno spajanje. Konstruirani su sklopovi s bočnim zupcima oblika V i W. Ispitivanjima na posmik malih uzoraka s različitim oblicima bočnih zubaca razvijen je kohezijski konstitucijski model s epoksidnim ljepilom koje je odabrano kao materijal za spajanje površine između zubaca. Spojna površina simulirana je epoksidnim ljepilom nulte debljine primjenom Voronoijevoga matematičkog modela za nasumičnu jediničnu podjelu. Ravninski mikromehanički simulacijski model konačnim elementima razvijen je primjenom računalnoga programa Abaqus za analizu oblika sloma i posmične čvrstoće šupljih ploča s dva sklopa s bočnim zupcima pod djelovanjem posmika, a za provjeru su provedena odgovarajuća ispitivanja na posmik. U sklopu s bočnim zupcima V oblika, vanjski beton je prvi izgubio čvrstoću te je isključen iz procesa, pri čemu je visina posmične površine pukotina kod potpunoga sloma bila približno polovina visine grede. Spoj s bočnim zupcima W oblika nije pokazao znatniji rani gubitak čvrstoće tijekom posmika, pri čemu je potpuna površina posmičnoga sloma iznosila približno 4/5 visine grede. Simulacijska analiza pokazala je veće širine pukotina tijekom sloma kod prvoga sklopa i manju širinu kod drugoga.

**Ključne riječi:**
šuplja ploča s bočnim zupcima, otpornost na posmik, kohezijska sila, konačni element, simulacijski eksperiment

## 1. Introduction

In current pre-fabricated hollow slab beams, the commonly used tongue-and-groove joint structure, as shown in Figure 1.a, has a transverse shear strength that is dependent on the height of the tongue-and-groove joint and the quality of the concrete inside the joint. Influenced by long-term overloading by vehicles during service, hollow slab bridges are prone to damage, such as steel reinforcement corrosion, joint failure, and beam cracking [1, 2]. Moreover, owing to insufficient height, the poor compactness of the concrete inside the joint, and fewer reinforcements, their shear strength is inherently low. When cracks and water ingress occur, the shear performance deteriorates rapidly, leading to severe stress on the individual slabs and endangering the safety of the main beam structure. These typical problems are receiving increasing attention, and studies on the shear resistance of joints are being increasingly conducted by domestic scientists. Wang [3] proposed a calculation method for the hinge joint shear force of slab–girder bridges using the energy method. The conclusion drawn in this study was that, as the number of slab–girder bridges increases, the hinge force increases, whereas the hinge force decreases as the span increases. Vellaichamy [4] studied the shear bonding capacity of composite plates featuring two distinct steel-cover plate profiles. The findings revealed that the predominant failure mode in the test samples was longitudinal shear failure between the concrete and profiled steel plates.

Gu et al. [5] analysed joint diseases by using finite element models, and established an evaluation system based on various disease parameters. Di et al. [6] conducted destructive tests on 12 in-service hollow slabs, and observed that the safety margin of the shear bearing capacity of hollow slab beams with a span of 10 m was only 5.3 %. Zhang et al. [7] conducted bending load tests on pre-stressed concrete hollow slab beams that have been in service for several years, and observed that their crack resistance significantly decreased with small stiffness and stress reserves. Wang et al. [8] innovatively used a membrane structure in finite element models to simulate the force transmission between joints. They proposed a lateral distribution calculation method considering the displacement between joints, confirming that the main cause of joint cracking between hollow slabs is the failure of the bonding interface between the joints and the hollow slabs. Zhou [9] first used shotcrete to reinforce slab bridges, and the reinforcement effect was good in actual bridge static load tests. Shotcrete can be used to reinforce slab beams and hinge joints in slab bridges. Demir [10] introduced an innovative approach for strengthening beams at the interaction points of adjacent structures, enabling design engineers to create reinforced concrete beam designs with these methods using straightforward calculations. Du et al. [11], through experiments and finite element simulation analysis, believed that the effect of cast-in-place concrete and joints on improving the shear bearing capacity of hollow slabs is limited, whereas the bonding slip between joints and hollow slab beams has limited influence on the shear bearing capacity. Scholars have proposed various reinforcement methods to solve these problems. Semendary et al. [12] used ultra-high-performance concrete as a joint-filling material to solve the early cracking problem of joints in American hollow-slab bridges, with good results in practical bridge applications. Zhong et al. [13] combined steel plates with steel fibre-reinforced polymers for hollow slab reinforcement, which significantly improved the bending bearing capacity and stiffness of hollow slab beams compared with the use of steel plates or steel fibre-reinforced polymers alone. Natarajan [14] observed that incorporating 0.09 % and 0.06 % glass fibres into concrete can effectively enhance its bending and shear strengths, which may help reinforce hinge joints. Zhang et al. [15] observed that the shear performance of side-reinforced ordinary concrete groove specimens was better than that of bottom-reinforced ordinary concrete groove specimens, and emphasised the significant influence of the casting direction on the shear strength of the bonding surface. Jin et al. [16] demonstrated that using anchor-type steel plates and concrete combined reinforcement under joint damage conditions can effectively restore the force transmission between simply supported hollow slabs, and significantly improve the overall stiffness of hollow slabs. Zhang [17] summarised the stress characteristics and failure mechanisms of hinge joints. They believed that increasing the size of hinge joints, augmenting and thickening hinge joint steel bars, enhancing the density of hinge joint steel bars, and adding hinge joint cross steel bars can effectively improve the force transmission performance and strengthen hinge joints.

Given the limited transverse shear strength between the existing tongue-and-groove hollow slabs, which is significantly lower than the shear strength of the beams themselves owing to the quality of the joints, some scholars have proposed changes in the construction of joints and hollow slabs to enhance the transverse shear strength. Zhang and Xue [18] proposed a novel type of hollow slab (mortise and tenon), as shown in Figure 1.b. The transverse connection of the new mortise-and-tenon hollow slab is theoretically superior to that of the commonly used tongue-and-groove joint. However, mortise-and-tenon construction requires joining adjacent beams starting from the beam end, which increases the construction difficulty. Following mortise-and-tenon assembly, an adhesive or grout needs to be injected to enhance the integrity. Ünal [19] conducted four-point bending tests on 16 reinforced concrete beams with a 1/1 scale by varying the shear span ratio/effective depth ratio (a/d) and stirrup spacing; the author observed that the a/d ratio and the number of stirrups have a significant influence on the performance of simply supported beams. Ye et al. [20] proposed improving the joint shear resistance by setting shear reinforcements at hollow slab joints. Feng [21] introduced a novel flange plate hollow-slab beam that economically outperformed conventional hollow slabs in a transverse connection in terms of construction and post-operation. Zhang et al. [22] experimentally demonstrated that the rough treatment of reserved grooves on the sides of hollow slabs not only enhanced the shear strength but also provided a certain level of ductility.

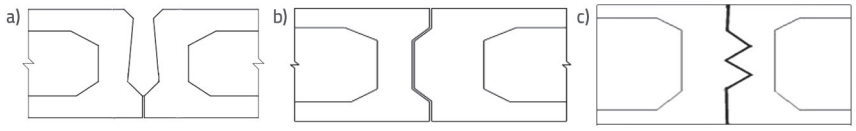


**Figure 1. Groove type, mortise-and-tenon, and lateral profile: a) Groove type; b) Mortise and tenon; c) Lateral profile**

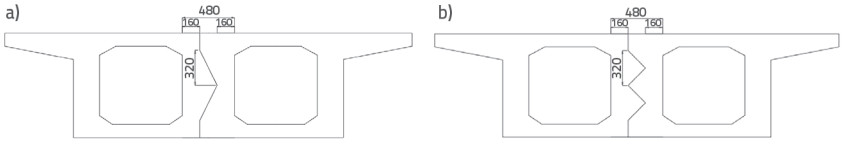


**Figure 2. Configuration of the proposed hollow slab: a) V-side tooth configuration; b) W-side tooth configuration**

The present authors suggest that a mortise-and-tenon hollow-slab structural system based on the concept of seamless joints can significantly enhance the contribution of the beam itself to the transverse shear strength. Therefore, the design of a new connection structure to maximise the transverse shear resistance is proposed. Accordingly, this paper presents a hollow slab structure with a side-toothed configuration for beam-to-beam bonding, as shown in Figure 1(c). Lateral interlocking increases the contribution of the beam to the shear resistance, and adhesive bonding simplifies construction compared with pouring tongue-and-groove wet joints. In contrast to the mortise-and-tenon construction, construction can commence from the middle beam, with subsequent beams joined sequentially from the beam side to eliminate construction difficulties. This study compares finite element simulation and experimental results to investigate the key shear parameters of the new hollow slab, the mechanical properties of structural adhesives, and the relationship between the side-tooth configuration and the inter-slab shear strength.

## 2. Design of connection structure for side-toothed hollow slabs

The design of the novel side-tooth structure involved a comparison of two types of teeth: V-side and W-side teeth. The tooth centre was positioned at the midpoint of the beam height, and the tooth depth (d) was designed to be 2/3 of the thickness (B) of the hollow slab web. The width of the V-side tooth (h) was designed to be three, four, and five times the tooth depth, whereas the total tooth width (h) of the W-side teeth was designed to be two, four, and six times the tooth depth. Referring to the standard drawing of pre-stressed hollow slabs with a span of 20 m and a beam height of 95 cm, with a web thickness (B) of 24 cm (including half the thickness of the tongue-and-groove joint), the corresponding dimensions of the side-toothed construction for the hollow slab are shown in Figure 2.

The sides of the beams (including the tooth surfaces and upper and lower vertical planes) were bonded using a structural adhesive. Following comparative assessments of the compressive strength, tensile strength, and aging resistance, two types of structural adhesives are recommended for bonding: epoxy and carbon plate adhesives. The mechanical performance indicators of both adhesives, measured after 168 h of normal curing and aging tests, are listed in Table 1.

## 3. Constitutive model of the materials

### 3.1. Constitutive model of concrete

This study aimed to establish a refined finite element simulation analysis model for the toothed connection structure of the side-toothed hollow slabs to analyse their shear performance. This requires adopting an appropriate and relatively precise constitutive model. Based on the stress characteristics of concrete within the tooth under the inter-beam shear force, the concrete shear constitutive model was established using the cohesive bilinear damage model in the Abaqus software. The constitutive model and mathematical function form are shown in Figure 3 and Eq. (1), respectively; the specific parameter results are listed in Table 2.

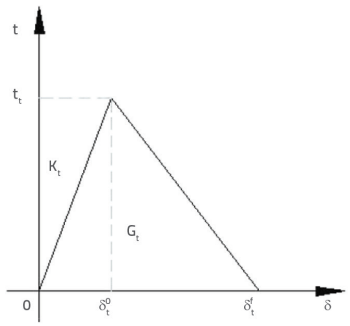


**Figure 3. Constitutive concrete model**

**Table 1. Mechanical performance indicators of the two types of structural adhesives**

| Mechanical performance / Adhesives | Tensile strength [MPa] | Aged tensile strength [MPa] | Average tensile strength aging rate [%] | Compressive strength [MPa] | Aged compressive strength [MPa] | Average compressive strength aging rate [%] |
|---|---|---|---|---|---|---|
| Carbon plate adhesive | 34.82 | 32.86 | 5.63 | 72.67 | 68.72 | 5.44 |
| Epoxy adhesive | 42.37 | 40.72 | 3.89 | 93.66 | 90.67 | 3.22 |

**Table 2. Material constitutive parameters**

| Material | $K_t$ [Pa/m] | $t_t$ [MPa] | $t_t^f$ [MPa] | $\delta_t^0$ | $\delta_t^u$ | $\delta_t^f$ | $G_t$ [J/m²] |
|---|---|---|---|---|---|---|---|
| Concrete | / | 1.95 | / | / | / | 4 | 15.60 |
| Epoxy adhesive-concrete | 0.39 | 2.68 | 1.98 | 7.10 | 7.89 | 10.62 | 16.76 |
| Carbon plate adhesive-concrete | 0.36 | 2.54 | 1.81 | 6.99 | 7.09 | 10.52 | 15.71 |

$$t = \begin{cases} K_t\delta \left(0 < \delta < \delta_t^0\right) \\ t_t \dfrac{\delta_t^f - \delta}{\delta_t^f - \delta_t^0} \left(\delta_t^0 < \delta < \delta_t^f\right) \end{cases} \quad (1)$$

$$t = \begin{cases} K_t\delta & 0 < \delta < \delta_t^0 \\ t_t^f + \left(t_t^m - t_t^f\right)\left(\dfrac{\delta_t^u - \delta}{\delta_t^u - \delta_t^0}\right) & \delta_t^0 < \delta < \delta_t^u \\ t_f & \delta_t^u < \delta < \delta_t^f \end{cases} \quad (2)$$

$K_t$ - Stiffness of the concrete specimens
$\delta$ - Shear displacement of the concrete specimens
$\delta_t^0$ - Displacement corresponding to the onset of damage (ultimate shear strength) of the concrete specimens
$\delta_t^f$ - Final cracking displacement of the concrete specimens
$t_t$ - Onset strength of damage (ultimate shear strength) of the concrete specimens
$G_t$ - Fracture energy

## 3.2. Shear constitutive model at the interface between structural adhesive and concrete

The shear constitutive models at the interface between the epoxy adhesive, carbon plate adhesive, and concrete were investigated using direct shear tests. Square specimens of C40 concrete prepared with two polished and cleaned side surfaces were bonded using a structural adhesive with a controlled adhesive layer thickness of 0.8–1.2 mm. After 168 h of curing, during which the adhesive achieved its design strength, the specimens were subjected to shear testing to determine the relationship between the shear force and the shear displacement. The experimental results were then used to fit the constitutive models, with the fitting principle ensuring consistent fracture energy. The final fitted results and mathematical form are shown in Figure 4 and Eq. (2), respectively.

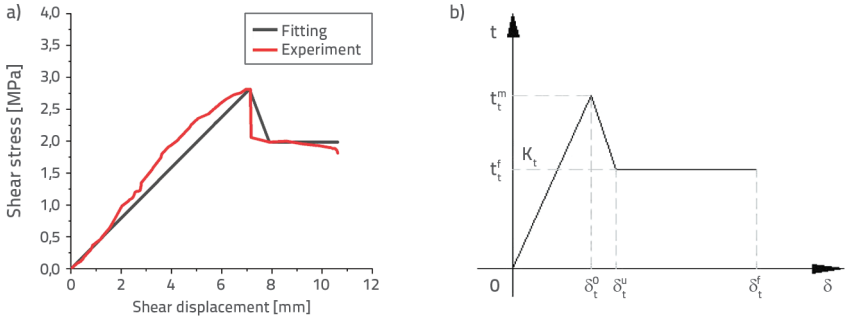


**Figure 4. Constitutive model of the structural adhesive: a) Fitting results; b) Constitutive model**

$K_t$ - Stiffness of the concrete specimens
$\delta$ - Shear displacement of the concrete specimens
$\delta_t^0$ - Displacement corresponding to the onset of damage (ultimate shear strength) of the concrete specimens
$\delta_t^f$ - Final cracking displacement of the concrete specimens
$t_t$ - Onset strength of damage (ultimate shear strength) of the concrete specimens
$G_t$ - Fracture energy
$\sigma_t^u$ - Strain corresponding to the stable phase of the tensile separation of the concrete specimens
$t_t^m$ - Onset strength of damage (ultimate shear strength) of the concrete specimens
$t_t^f$ - Stable strength during the tensile separation phase of the concrete specimens.

## 3.3. Design of shear test specimen

In the shear test specimens described in a later section, the hollow portion within the slab was simplified, that is, no hollow space was incorporated. The design schematic of the specimens and actual specimen photograph are shown in Figure 5.

This study fabricated 30 sets of specimens, namely, 10 sets of unbonded specimens, 10 sets of bonded specimens with the carbon plate adhesive, and 10 sets of bonded specimens with the steel adhesive, with three specimens in each set. For each type of straight line, V-side teeth, and W-side teeth, the arithmetic mean of 10 sets of test results was calculated. The experiment began by bonding concrete specimens of various tooth shapes with the carbon plate or steel adhesive, placing them on the testing equipment, and controlling the vertical load using a computer. Initially, the lateral pressure was increased to 0.5 kN at a rate of 200 N/s, and then to 10 MPa at a rate of 100 N/s. Once the vertical loading was completed, the direction was switched to horizontal shear. The horizontal loading was

**Table 3. Shear test results of concrete specimens with different tooth shapes along the 'bonding surface'**

| Serial number | Shape | Non-cementing [MPa] | Carbon plate cement [MPa] | Steel adhesive bond [MPa] |
|---|---|---|---|---|
| 1 | Straight line | 2.03 | 2.49 | 2.68 |
| 2 | V-side teeth | 2.26 | 2.89 | 3.07 |
| 3 | W-side teeth | 2.46 | 3.03 | 3.66 |

controlled by the displacement, starting with a trial load of 0.1 mm. Once the trial loading was completed, the main loading was initiated at a rate of 1 mm/s until the specimen failed. If data anomalies were detected during the test, the loading was halted immediately until the issue was resolved, before resuming. The final shear strength test results for the specimens with various tooth shapes using the two different bonding materials are presented in Table 3.

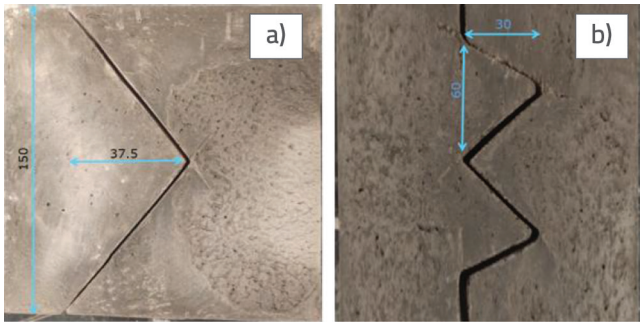


**Figure 5. Specimen drawing: a) V-side teeth; b) W-side teeth**

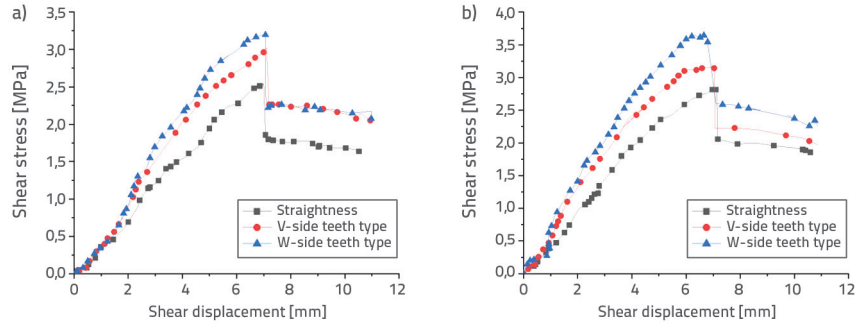


**Figure 6. Shear results of specimens with different tooth shapes with the carbon plate adhesive and steel adhesive: a) Carbon plate adhesive; b) Steel adhesive**

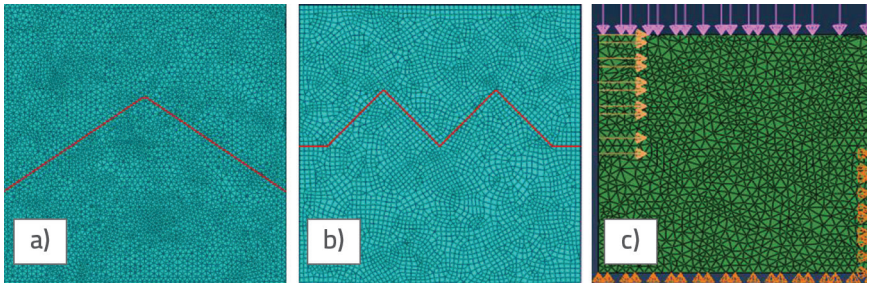


**Figure 7. Model and simulation loading diagrams: a) V-side teeth; b) W-side teeth; c) Loading graph**

Under the condition of the same shape of the test block, whether the shape of the test block was straight, V-side teeth, or W-side teeth, the shear strength of the concrete test block filled with the steel adhesive was higher than that filled with the carbon plate adhesive. Under the same packing conditions, the shape of the test block varied from a straight line to a W-side tooth shape, and the shear strengths of the test block sandwich concrete, carbon plate adhesive, and steel adhesive increased successively. After comprehensive consideration, it was concluded that the shear strength of the W-side-teeth-shaped specimen with the steel adhesive was the highest, and the shear effect was the best.

Figure 6 shows the relationship between the shear displacement and shear stress of concrete with different shapes with the carbon plate adhesive and steel adhesive.

## 4. Finite element simulation analysis of lateral tooth shear specimen

The vertical force transfer shear problem is a plane stress problem; thus, a plane model was developed. In this study, the Abaqus software was used to develop the V-side and W-side teeth specimen models of the steel adhesive. In these models, the concrete adopted a two-dimensional plane strain (CPE3) unit, the interfacial interlayer was a steel adhesive, a two-dimensional four-node bond unit (COH2D4) was considered, and the property was set as a thickless cohesive unit. A simulation and analysis model of a scaled structure was developed to facilitate the comparison, verification, and parameter correction with subsequent scaled shear tests.

As shown in Figure 7, when testing the shear strength, a low lateral pressure (compaction interface action) was applied. The model was consistent with the experimental load and boundary conditions. A load control size of 45 kN (purple arrows in Figure 7.c) was adopted at the upper end of the model to simulate the side pressure. The bottom of the model constrained the displacement in the Y-direction, the right end constrained

the displacement in the X-direction, and the horizontal load was applied to the half-height range of the left surface to form the wrong shear force. The application of the horizontal shear force was controlled by a maximum horizontal displacement of 25 mm, and the loading step length was 0.0001 steps in the Abaqus analysis. The developed specimen model and schematic of the simulated loading are shown in Figure 7.

### 4.1. Results of finite element simulation

The results obtained from finite element simulation are shown in Figures 8 and 9. As evident from Figures 8, 9.a and 9.b, when the test block was subjected to a compressive shear force, the largest deformation occurred at the cementation boundary, that is, the part circled in the figure. However, because of the viscosity of the cementation material itself, neither the V-side nor the W-side teeth unhinged test blocks failed first. The concrete part at the red dotted line in the figure was likely to be the first to fail under the compressive shear force, and the failure form of the actual test block was consistent with the simulation process. When the unhinged test block was the V-side teeth type, the shear strength increased by approximately 35.8 % compared with that of ordinary concrete joints. When the unhinged test block was the W-side teeth type, the shear strength was 48.8 % higher than that of the ordinary concrete hinge joints, indicating that the shear strength of the W-side-tooth-shaped test block was higher than that of the V-side-tooth-shaped test block when the filler was the steel adhesive.

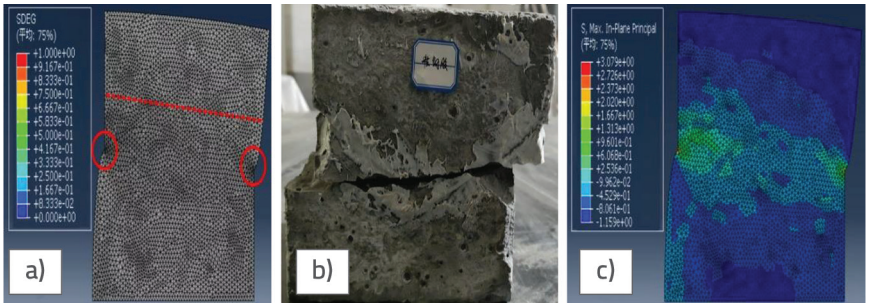


**Figure 8. Comparison of the test and simulation results for the V-side tooth with the steel adhesive: a) Stiffness cracking; b) Test cracking; c) Shearing stress**

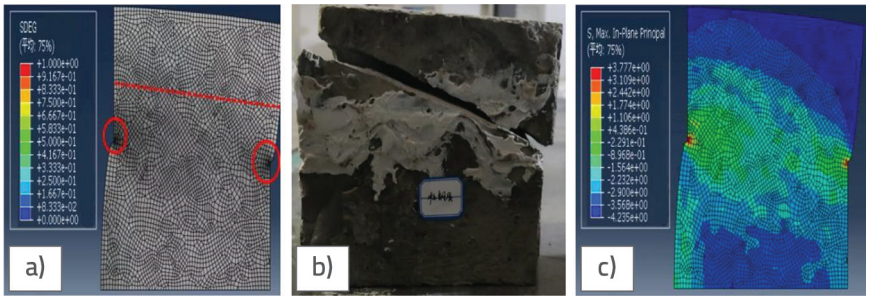


**Figure 9. Comparison of the test and simulation results for the W-side tooth with the steel adhesive: a) Stiffness cracking; b) Test cracking; c) Shearing stress**

The numerical simulation results are shown in Figures 8 and 9.c. Table 4 presents a comparison of the simulated and experimental results. When the unhinged test block was the V-side teeth type, the shear strength of the real test block was 3.07 MPa, whereas that obtained in the numerical simulation was 3.08 MPa; the error between the two was only 0.3 %. When the unhinged test block was the W-side teeth type, the shear strength of the real test block was 3.72 MPa, whereas that obtained in the numerical simulation was 3.78 MPa; the error between the two was only 1.6 %, indicating that the two results are highly consistent with each other. Thus, the highest shear strength was obtained using the steel adhesive.

**Table 4. Comparison of the simulated and experimental shear values**

| Serial number | Shape | Test result [MPa] | Simulation result [MPa] | Error [%] |
|---|---|---|---|---|
| 1 | V-side teeth | 3.07 | 3.08 | 0.3 |
| 2 | W-side teeth | 3.66 | 3.78 | 1.6 |

According to the comprehensive test and simulation results, the shear strength of the test piece can be significantly improved using the W-side teeth shape connected using the steel adhesive. Therefore, the new hinge joint can be considered to improve the shear strength of hollow slab beams.

## 5. Conclusion

To maximise the transverse shear resistance, a cemented lateral tooth hollow-slab structure was proposed.

The strength and aging properties of four types of cementing materials were compared, and the best cementing material suitable for these structures was determined to be a steel adhesive.

Based on a linear experiment, a cohesive force–shear constitutive model of the steel adhesive was proposed, and the corresponding constitutive parameters were determined. Based on a side-tooth structure experiment, it was shown that the non-hinged W-side teeth joint with the steel adhesive could significantly improve the overall shear performance of the structure and effectively improve the overall stiffness of the hollow slab. The corresponding failure surface was also improved,

cracking not only along the interface of the hinged joint, but also along the interface of the hinged joint. The hollow slab also cracked, which improved the shear cracking mode of the hinged joint to some extent.

A cohesive force element finite element model was developed. The simulation results were consistent with the test data, indicating that the design could accurately achieve the maximum transverse shear resistance, and that the stress process and failure modes were conducive to the improvement of the shear resistance.

## Acknowledgements

This study was financially supported by the National Natural Science Foundation of China (grant no. 52178285). The authors gratefully acknowledge this support.

## REFERENCES

[1] Aimin, Y., Ji, B., Di, H.: Countermeasure for the typical damage of prestressed concrete hollow slab girder, GeoHunan International Conference, Hunan, China.

[2] Naito, C., Jones, L., Hodgson, I.: Development of flexural strength rating procedures for adjacent prestressed concrete box girder bridges, Journal of Bridge Engineering, (2011), pp. 662-670. https://doi.org/10.1061/(ASCE)BE.1943-5592.0000186

[3] Gang, W.: Strength analysis of shear joints in articulated plate beam bridges, Journal of Shanghai Institute of Railway Technology, 15 (1994) 3, pp. 20-25.

[4] Vellaichamy, P., Veerasamy, S., Mangottiri, V.: Shear Bond Characteristics of Steel Concrete Composite Deck Slab, GRAĐEVINAR, 74 (2022) 5, pp. 393-401, https://doi.org/10.14256/JCE.3273.2021

[5] Gu, W.: Research on hinge joint damage evolution rule and evaluation Technology of Concrete Hollow Slab Girder Bridge, Yangzhou University, Yangzhou, China, 2020.

[6] Di, J., Sun, Y., Yu, K., et al.: Experimental Investigation of Shear Performance of Existing PC Hollow Slab, Engineering Structures, (2020), pp. 211. https://doi.org/10.1016/j.engstruct.2020.110451

[7] Wang, J., Zhang, G., Liu, J., et al.: Research on destructive test of pretensioned prestressed concrete hollow slab in service, International Journal of Structural Integrity, (2018), pp. 211. https://doi.org/10.1108/IJSI-07-2017-0043

[8] Gang, W.: Mechanism analysis on typical diseases of prestressed concrete hollow core slab bridges, Zhejiang University, Zhejiang, China, 2016.

[9] Zhou, X.D.: Study on the Application of Shotcrete in Reinforcing Slab Bridges, Chang'an University, Shanxi, China, 2005.

[10] Demir, A., Ince, Y., Altıok, T.Y.: Experimental and Numerical Investigation of RC Beams Strengthened with CFRP Composites, GRAĐEVINAR, 73 (2021) 6, pp. 605-616, https://doi.org/10.14256/JCE.3051.2020

[11] Menglin, D., Zhouhong, Z., Yuchen, L., et al.: Shear Bearing Performance of Prestressed Concrete Hollow Slab Beams in Service, Journal of Southeast University, 51 (2021) 3, pp. 384-390.

[12] Semendary, A.A.: Early age behaviour of an adjacent prestressed concrete box-beam bridge containing UHPC shear keys with transverse dowels, Journal of Bridge Engineering, (2017). https://doi.org/10.1061/(ASCE)BE.1943-5592.0001034

[13] Zhong, X.Q.: Theoretical and experimental research on hollow slab beam bridge reinforced by steel plate and fibre-modified Polymer Concrete, Harbin Institute of Technology, Heilongjiang, China, 2019.

[14] Natarajan, S., Murugesan, A., Dhanapal, J., Narayanan, A.: Glass fibre reinforced ultra-high strength concrete with silica fume, GRAĐEVINAR, 74 (2022) 10, pp. 849-856, https://doi.org/10.14256/JCE.3431.2021

[15] Tao, Z.: Experimental study on shear resistance of bond surface of new and old concrete under the Influence of Many Factors, Hunan Agricultural University, Hunan, China, 2019.

[16] Hui, J.: Test and Calculation Method of Anchor Steel-Concrete Reinforcement Technology for Strengthening Prefabricated Hollow Slab Bridge, Chang'an University, Shanxi, China, 2021.

[17] Zhi, Z.: Hollow plate hinge seam failure mechanism and prevention measure research, Shanxi Architecture, 35 (2009) 2, pp. 318-320.

[18] Xiaowan, Z.: Precast hollow-cored slab bridge transverse joint Design and Improvement Methods, Jilin University, Jilin, China, 2017.

[19] Ünal, A., Kamanlı, M., Solak, A., Cengiz, S.: Numerical investigation of the effect of support conditions on beam shear behaviour in full scale reinforced concrete beams, GRAĐEVINAR, 75 (2023) 12, pp. 1193-1201, https://doi.org/10.14256/JCE.3823.2023

[20] Jian-Shu, Y., Jiu-Sheng, L., Bo, Y., et al.: Experiment on Shear Property of Hinge Joints of Concrete Hollow Slab, Journal of Highway and Transportation Research and Development, 30 (2013) 6, pp. 33-39.

[21] Shuang, F.: Study on transverse structure Optimization of Prestressed Concrete Hollow Slab Beams, Harbin Institute of Technology, Heilongjiang, 2020.

[22] Juan-Xiu, Z., Jun, L., Jian-Shu, Y., et al.: Study on Surface Roughness Treatment of Hollow Panel Side, Journal of China & Foreign Highway, 33 (2013) 6, pp. 136-139, https://doi.org/10.14048/j.issn.1671-2579.2013.06.031